Constraints on an empirical equation for asymmetry-induced transport

D. L. Eggleston
Department of Physics, Occidental College, Los Angeles, California 90041, USA

(Received 1 December 2009; accepted 15 March 2010; published online 13 April 2010)

Previous work on asymmetry-induced transport in a modified Malmberg–Penning trap showed that the radial particle flux was empirically constrained to be of the form $\Gamma(\epsilon)=-(B_0/B)^{1.33}D(\epsilon)[\nabla n_0+f(\epsilon)]$, where $\epsilon=\omega-l\omega_R$, $\omega_R(r)=v_\theta/r$ is the column rotation frequency, ω and l are the asymmetry frequency and azimuthal mode number, ∇n_0 is the radial density gradient, B is the magnetic field, B_0 is an empirical constant, and $D(\epsilon)$ and $f(\epsilon)$ are unknown functions. In this paper, it is shown that further constraints can be placed upon $D(\epsilon)$ and $f(\epsilon)$ by comparing data near the $\epsilon=0$ points to a first order expansion of $\Gamma(\epsilon)$. It is shown that $dD/d\epsilon(0)\neq 0$, in contradiction to resonant particle theory, and that $f(\epsilon)$ can only be a fraction of the size predicted by that theory. Finally, it is shown that $dD/d\epsilon(0)$ exhibits a power-law scaling with radius, magnetic field, and the bias of the center conductor of the trap. © *2010 American Institute of Physics*. [doi:10.1063/1.3381069]

I. INTRODUCTION

Asymmetry-induced radial particle transport in cylindrical Malmberg–Penning non-neutral plasma traps has been studied for over 25 years by several research groups.[1–8] Despite the simplicity of these traps, a full understanding of the transport remains elusive, and there is little agreement between experiments and theory. Indeed, our previous work in a modified version[9] of these traps designed specifically to test resonant particle transport theory[10] revealed serious discrepancies between experiments and this theory.[11] In particular, the experimental dependence of the transport on asymmetry frequency ω was both quantitatively and qualitatively different than the predictions of theory. However, it was not clear from these experiments which part(s) of the theory were in error.

In a previous paper,[12] we presented a new approach to the study of asymmetry-induced transport based on the hypothesis that the asymmetry frequency ω and the plasma rotation frequency ω_R always enter the physics in the combination $\omega-l\omega_R$, where l is the azimuthal mode number of the asymmetry. This hypothesis was suggested by the appearance of this combination in theories for various phenomena in non-neutral plasmas. In order to simplify the data analysis, it proved useful to focus on data points where this combination was zero. From our typical measurements of the radial particle flux Γ versus radius r, we selected the flux Γ_{sel} at the radius where $\omega-l\omega_R=0$. By independently varying ω, ω_R, and the magnetic field B, we showed that Γ_{sel}, for a fixed asymmetry amplitude, satisfied the equation

$$\Gamma_{\text{sel}}=-(B_0/B)^{1.33}D_0[\nabla n_0+f_0], \tag{1}$$

where ∇n_0 is the radial density gradient, and $B_0=233$ G, $D_0=1.00$ cm^2 s^{-1}, and $f_0=-1.01\times10^5$ cm^{-4} are empirical constants. Although this equation only gave the flux for points where $\omega-l\omega_R=0$, we also deduced the form of the general flux equation. Our data analysis revealed that the expression for the general flux Γ must be a function of the combination $\omega-l\omega_R$. In addition, the general flux expression had to reduce to the equation for Γ_{sel} when $\omega-l\omega_R=0$. Without further information, we thus allowed both D_0 and f_0 to become functions of $\epsilon\equiv\omega-l\omega_R$, obtaining

$$\Gamma(\epsilon)=-(B_0/B)^{1.33}D(\epsilon)[\nabla n_0+f(\epsilon)], \tag{2}$$

where $D(\epsilon)$ and $f(\epsilon)$ are unknown functions and $D(\epsilon=0)\equiv D_0$ and $f(\epsilon=0)\equiv f_0$.

While Eq. (2) appears as a slight modification of Eq. (1), the consideration of nonzero ϵ opens the possibility for additional parametric dependences that do not appear in Eq. (1) if these parameters appear in a product or quotient with ϵ. For example, if ϵ is scaled to the cyclotron frequency ω_c (i.e., if it appears as ϵ/ω_c), this would introduce an additional dependence on B not captured in the $B^{-1.33}$ scaling of Eq. (1). Similarly, if ϵ appears scaled to ω_R, then our initial hypothesis about the rotation frequency only appearing in the combination $\omega-l\omega_R$ will have to be modified.

The magnetic field dependence of Eq. (2) does not match that given by resonant particle transport theory in either the plateau or banana regimes. The rest of the equation, however, is compatible with that theory. In particular, the theory gives, for either regime,

$$f(\epsilon)=\frac{n_0}{T}\frac{dT}{dr}\left(\frac{\epsilon^2}{2k^2\bar{v}^2}-\frac{1}{2}\right)+\frac{rn_0\omega_c\epsilon}{l\bar{v}^2}, \tag{3}$$

while $D(\epsilon)=\tilde{D}\exp(-\epsilon^2/2k^2\bar{v}^2)$, where k is the axial wavenumber of the asymmetry, $\bar{v}$ is the thermal velocity, ω_c is the cyclotron frequency, and $\tilde{D}$ depends on the regime.

In this paper, we show that further empirical constraints can be placed on $D(\epsilon)$ and $f(\epsilon)$ by examining data points adjacent to the $\epsilon=0$ points and comparing them to a first order expansion of $\Gamma(\epsilon)$. In particular, we show that $dD/d\epsilon(0)\neq 0$, which excludes $D(\epsilon)$ of the form given by resonant particle theory. Further, we show that Eq. (3) is also incompatible with the data unless it is reduced in magnitude. Finally, we show that $dD/d\epsilon(0)$ has power-law dependences on r, B, and the center wire bias ϕ_{cw}.

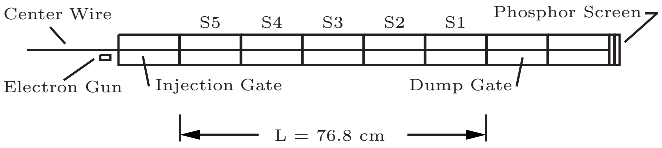

FIG. 1. Schematic of the Occidental College Trap. The usual plasma column is replaced by a biased wire to produce the basic dynamical motions in low density electrons injected from an off-axis gun. The low density and high temperature of the injected electrons largely eliminate collective modifications of the vacuum asymmetry potential. The five cylinders (labeled S1–S5) are divided azimuthally into eight sectors each.

II. LINEARIZATION

We start by performing an expansion of Eq. (2) for small values of ϵ. The expansions for $D(\epsilon)$ and $f(\epsilon)$ are

$$D(\epsilon) = D(0) + \epsilon \frac{dD}{d\epsilon}(0) + \frac{\epsilon^2}{2}\frac{d^2D}{d\epsilon^2}(0) + \cdots \tag{4}$$

and

$$f(\epsilon) = f(0) + \epsilon \frac{df}{d\epsilon}(0) + \frac{\epsilon^2}{2}\frac{d^2f}{d\epsilon^2}(0) + \cdots . \tag{5}$$

Using these in Eq. (2), we obtain, to first order in ϵ,

$$\Gamma = -\left(\frac{B_0}{B}\right)^{1.33}\left\{ D_0[\nabla n_0 + f_0] + \epsilon\left[(\nabla n_0 + f_0)\frac{dD}{d\epsilon}(0) + D_0 \frac{df}{d\epsilon}(0)\right]\right\}, \tag{6}$$

where we have used the equivalent notations $D(\epsilon{=}0)=D_0$ and $f(\epsilon{=}0)=f_0$. Any variation in parameters Ω multiplying ϵ will be higher order in ϵ since $d(\epsilon\Omega)=\Omega d\epsilon+\epsilon d\Omega$. Noting that the zeroth-order term in the expansion is Γ_{sel}, as given by Eq. (1), we move this term to the left hand side. Taking the derivative with respect to ϵ we obtain

$$\frac{d(\Gamma - \Gamma_{\mathrm{sel}})}{d\epsilon} = -\left(\frac{B_0}{B}\right)^{1.33}\left[(\nabla n_0 + f_0)\frac{dD}{d\epsilon}(0) + D_0 \frac{df}{d\epsilon}(0)\right]. \tag{7}$$

From this result, we can see that since ∇n_0, D_0, and f_0 are known, we may be able to obtain information about $(dD/d\epsilon)(0)$ and $(df/d\epsilon)(0)$ by examining the experimental values of $[d(\Gamma-\Gamma_{\mathrm{sel}})]/d\epsilon$ for small ϵ.

III. EXPERIMENTAL APPARATUS

Our transport studies are performed in the modified Malmberg–Penning trap shown in shown in Fig. 1. As in the standard trap design, a uniform axial magnetic field B provides radial confinement of injected electrons, while negatively biased end cylinders (the injection gate and dump gate) provide axial confinement. Our device also operates in the standard inject-hold-dump cycle. A cycle begins by grounding the injection gate which allows electrons from the gun to flow into the central region. This injection gate is then returned to a negative bias which traps the electrons. After a chosen period of time, the dump gate is grounded and the electrons leave the trap and hit a positively biased phosphor screen. Analysis of the images on this screen provides the primary diagnostic.

The principal modification in our device is replacing the usual plasma column with a biased wire running along the axis of the trap. The wire provides a radial electric field to replace the field normally produced by the plasma column and allows the injected low density electrons to have the same zeroth-order dynamical motions (axial bounce and azimuthal $E\times B$ drift motions) as in a standard trap. The lower density ($10^5\ \mathrm{cm}^{-3}$) and high temperature (4 eV) of the electrons give a Debye length larger than the trap radius. Under these conditions, potentials in the plasma are essentially the vacuum potentials and previously encountered[2] complications due to collective effects are minimized.[11] Our design also allows the drift rotation frequency $\omega_R(r)$ to be easily adjusted by varying the center wire bias ϕ_{cw} since

$$\omega_R = \frac{-\phi_{cw}}{r^2 B \ln(R/a)}, \tag{8}$$

where R and a are the radii of the wall and the center wire, respectively. Despite these changes, the unperturbed confinement time has similar magnitude and shows[9] the same $(L/B)^2$ scaling found in higher density experiments, thus supporting the idea that the radial transport is primarily a single particle process and confirming the relevance of our experiments to standard trap physics.

A unique feature of our device is that the entire confinement region is sectored (five cylinders, labeled S1 through S5 in Fig. 1, with eight azimuthal divisions each). This allows us to apply a simple, known asymmetry by selecting the amplitude and phase of the voltages applied to each sector to produce a helical standing wave of the form

$$\phi(r,\theta,z,t) = \phi_W\left(\frac{r}{R}\right)^l \cos\left(\frac{n\pi z}{L}\right)\cos(l\theta - \omega t), \tag{9}$$

where ϕ_W is the asymmetry potential at the wall (typically 0.2 V), R is the wall radius (3.82 cm), L is the length of the confinement region (76.8 cm), n and l are the axial and azimuthal Fourier mode numbers, respectively, and here z is measured from one end of the confinement region. For these experiments $n=l=1$ and the relative phases of the applied voltages are adjusted so that the asymmetry rotates in the same direction as the zeroth-order azimuthal $E\times B$ drift. For these experiments, the higher order harmonics of the applied asymmetry have amplitudes less than 10% of the fundamental. Since the transport typically scales like the square of the asymmetry amplitude,[13] the effect of these harmonics can be ignored.

Data acquisition for these transport studies can be summarized as follows; details have been given elsewhere.[11,13] Electrons injected into the trap from an off-axis gun are quickly dispersed into an annular distribution. At a chosen time (here, 1600 ms after injection), the asymmetries are switched on for a period of time δt (here, 100 ms) and then switched off. At the end of the experiment cycle, the electrons are dumped axially onto a phosphor screen and the resulting image is digitized using a 512×512 pixel charge-

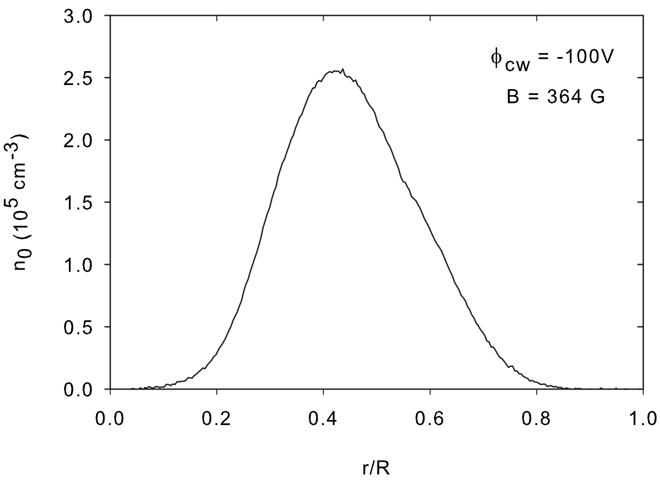

FIG. 2. A typical density profile taken 1600 ms after injection.

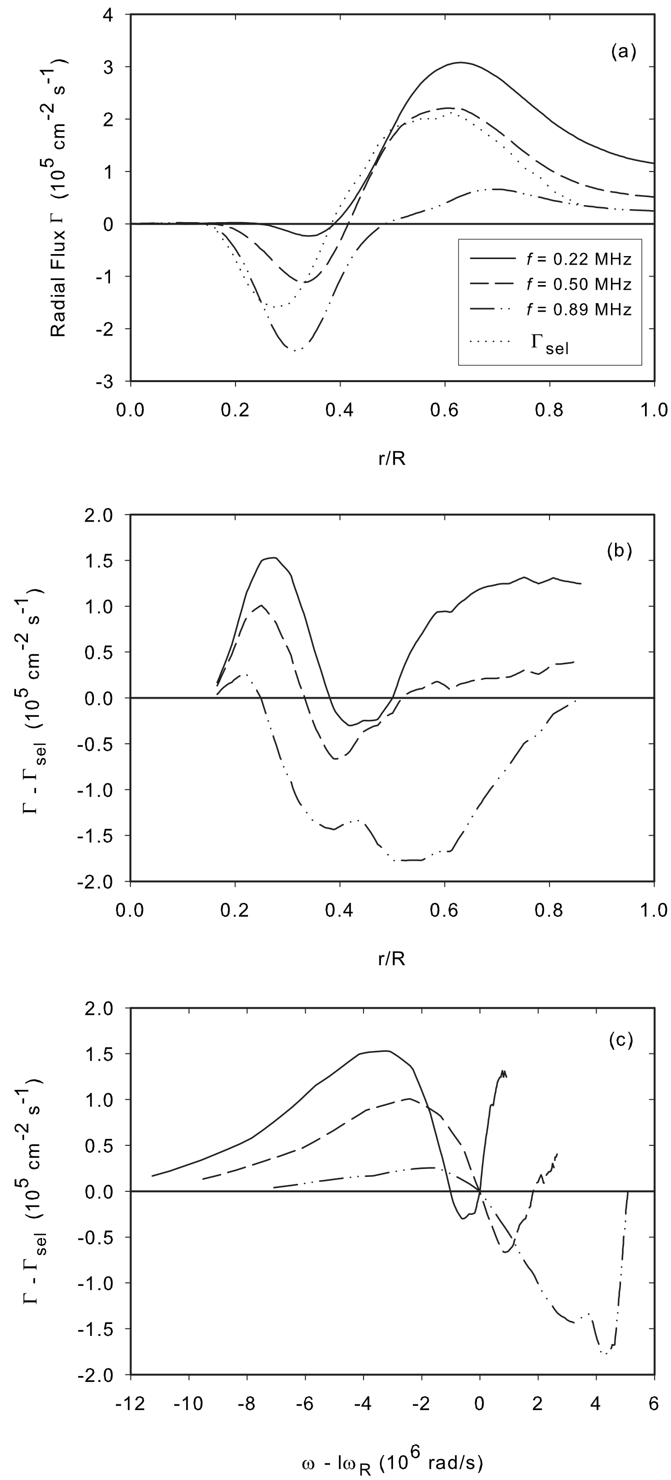

FIG. 3. Procedure for analyzing the data. (a) Radial flux Γ vs scaled radius r/R for three representative asymmetry frequencies. Each of the 26 frequencies contributes one point to the Γ_{sel} curve. For this data, $B=364$ G and $\phi_{cw}=-100$ V. (b) The difference $\Gamma-\Gamma_{sel}$ vs r/R for the same three representative frequencies. (c) The radius values in (b) are mapped to the corresponding values of $\omega-l\omega_R$ to produce this plot. The slope of these curves at the origin is used to obtain the left hand side of Eq. (7).

coupled device camera. A radial cut through this image gives the density profile $n_0(r)$ of the electrons. A typical profile is shown in Fig. 2. Shot-to-shot variation in the number of injected electrons is less than 1% and the data is very reproducible. Calibration is provided by a measurement of the total charge being dumped. Profiles are taken both with the asymmetry on and off, and the resulting change in density $\delta n_0(r)$ is obtained. The background transport is typically small compared to the induced transport and is subtracted off. If the asymmetry amplitude is small enough and the asymmetry pulse length δt short enough, then $\delta n_0(r)$ will increase linearly in time.[13] We may then approximate $dn_0/dt \simeq \delta n_0(r)/\delta t$ and calculate the radial particle flux $\Gamma(r)$ [assuming $\Gamma(r=a)=0$]:

$$\Gamma(r) = -\frac{1}{r}\int_a^r r' dr' \cdot \frac{dn_0}{dt}(r'). \quad (10)$$

Here a is the radius of the central wire (0.178 mm). The entire experiment is then repeated for a series of asymmetry frequencies ω and the resulting flux versus radius and frequency data saved for analysis.

IV. RESULTS

In order to compare our data with Eq. (7), we need to transform our flux data from the usual Γ versus r form to $\Gamma-\Gamma_{sel}$ versus ϵ. The procedure has several steps but is straightforward and is illustrated in Fig. 3. We first obtain a set of flux versus radius data for a number of asymmetry frequencies ω (typically 26) as discussed in Sec. III. Typical Γ versus r plots are shown in Fig. 3(a) for three of these frequencies. For this illustrative data $B=364$ G and $\phi_{cw}=-100$ V. For each plot there is one radial point where the asymmetry frequency matches the rotation frequency, i.e., $\omega=l\omega_R$. The value of Γ at this point is used to construct the Γ_{sel} curve. When this process is repeated for the full set of asymmetry frequencies, the Γ_{sel} versus r curve shown by the dotted line is obtained. It is worth noting that the data for the three curves vary smoothly through the $\epsilon=0$ point where they cross the Γ_{sel} curve. This insures that the derivative with respect to ϵ taken at the end of the data analysis will not give a peculiar result. Now the $\Gamma-\Gamma_{sel}$ curves shown in Fig. 3(b) can be constructed by subtracting $\Gamma_{sel}(r)$ from each of the $\Gamma(r)$ curves. Finally, we use Eq. (8) to map the radii in Fig. 3(b) to the corresponding values of $\omega-l\omega_R$, again doing this

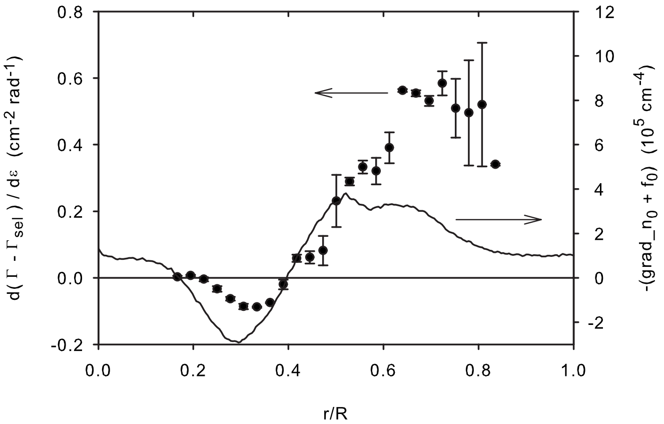

FIG. 4. The black dots in this figure show $d(\Gamma-\Gamma_{\text{sel}})/d\epsilon$ vs the scaled radius r/R. The scale for this data is on the left. The solid line shows $-(\nabla n_0+f_0)$ vs r/R for comparison. The scale for this data is on the right. Note that both data sets cross the zero axis at $r/R\approx 0.4$.

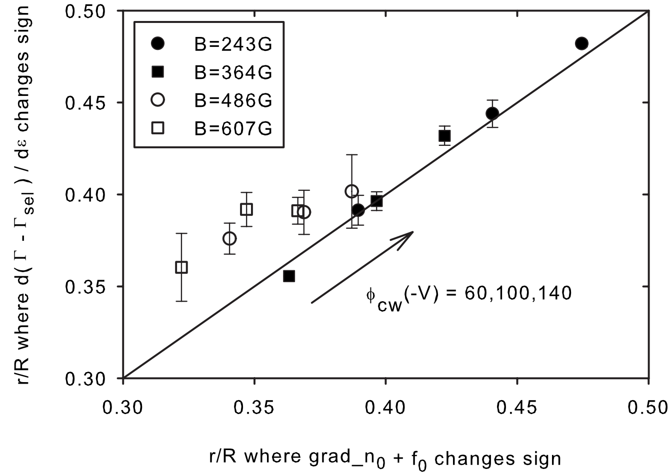

FIG. 5. Correlation in zero crossing of $d(\Gamma-\Gamma_{\text{sel}})/d\epsilon$ and (∇n_0+f_0) with magnetic field B and center wire bias ϕ_{cw} as parameters. The solid line shows where the data would lie if the correlation were perfect.

separately for each asymmetry frequency. For our representative cases this yields the $\Gamma-\Gamma_{\text{sel}}$ versus $\omega-l\omega_R$ curves shown in Fig. 3(c). We then find the slope of these curves at the point where they pass through the origin to obtain $d(\Gamma-\Gamma_{\text{sel}})/d\epsilon$ for small ϵ. These values are then plotted versus the radius at which $\epsilon=0$. Repeating this process for all the asymmetry frequencies produces the black dots in Fig. 4.

To estimate the uncertainty in $d(\Gamma-\Gamma_{\text{sel}})/d\epsilon$, we have obtained this quantity in two ways. First, we simply take one data point on either side of $\epsilon=0$ and approximate $d(\Gamma-\Gamma_{\text{sel}})/d\epsilon\approx\Delta(\Gamma-\Gamma_{\text{sel}})/\Delta\epsilon$. Second, we take three data points on either side of $\epsilon=0$, fit a second order polynomial to the data, and use the linear coefficient for $d(\Gamma-\Gamma_{\text{sel}})/d\epsilon$. We used the result of this latter procedure for the data points and the difference between the two procedures for the uncertainty.

Given the form of Eq. (7), it is instructive to compare the data points in Fig. 4 with the data for $-(\nabla n_0+f_0)$, and this latter quantity is shown by the solid line. Note that both the black dots and the solid line have a zero-crossing at essentially the same radius. Since most quantities that enter the physics do not change sign with radius, this suggests that the first term in Eq. (7) is dominant, at least in the vicinity of the zero-crossing radius. This conclusion is supported when the experimental parameters are varied. Varying the magnetic field B and the center wire bias ϕ_{cw}, we obtain results similar to Fig. 4 and shifts in the zero-crossing of $-(\nabla n_0+f_0)$ (due to the variation in parameters) are tracked by the zero-crossing of $d(\Gamma-\Gamma_{\text{sel}})/d\epsilon$. This correlation is shown in Fig. 5 where the ordinate gives the scaled radius r/R where $d(\Gamma-\Gamma_{\text{sel}})/d\epsilon$ changes sign and the abscissa gives the scaled radius where $-(\nabla n_0+f_0)$ changes sign. The uncertainties stem from the uncertainties in the data plots such as that of Fig. 4. Data are given for three values of the center wire bias ϕ_{cw} for each of four magnetic fields B, with the higher absolute values of ϕ_{cw} giving zero-crossings at larger r/R as indicated by the arrow.

The observed correlation allows us to restrict the form of the unknown function $D(\epsilon)$. Referring to Eq. (7), we see that the correlation requires that $dD/d\epsilon(0)\neq 0$. This is noteworthy since it excludes $D(\epsilon)$ of the form found in resonant particle transport theory.[11] In this theory, $D(\epsilon)\propto\exp(-\epsilon^2/2k^2\bar{v}^2)$ and thus $dD/d\epsilon(0)=0$. Here $k=n\pi/L$ is the axial mode number.

The correlation between zero-crossings also shows that the form of $f(\epsilon)$ given by resonant particle theory is incorrect. According to the theory, for either the plateau or banana regimes, $f(\epsilon)$ is given by Eq. (3) and thus

$$\frac{df}{d\epsilon}(0)=\frac{rn_0\omega_c}{l\bar{v}^2}. \tag{11}$$

The effect of including such a term is shown in Fig. 6. Using experimental values in Eq. (11) we obtain the curve for $D_0(df/d\epsilon)(0)$ shown in Fig. 6(a). Since we do not know $(df/d\epsilon)(0)$, we move $D_0(df/d\epsilon)(0)$ to the left hand side of Eq. (7):

$$\left(\frac{B}{B_0}\right)^{1.33}\frac{d(\Gamma-\Gamma_{\text{sel}})}{d\epsilon}+D_0\frac{df}{d\epsilon}(0)=-(\nabla n_0+f_0)\frac{dD}{d\epsilon}(0). \tag{12}$$

Figure 6(b) shows the effect of including the $D_0(df/d\epsilon)(0)$ term. The lower line shows the same data plotted as dots in Fig. 4 multiplied by the constant $(B/B_0)^{1.33}$. We have interpolated the data between the points to allow for easy addition of the $D_0(df/d\epsilon)(0)$ data which includes 256 radial values. The upper line shows the effect of this addition. In this case, the curve is shifted upward enough so that there is no longer a zero-crossing. Since we know that the right side of Eq. (12) crosses zero at roughly $r/R=0.4$, we have a contradiction. Thus, $D_0(df/d\epsilon)(0)$ cannot be given by Eq. (11).

It is tempting at this point to conclude that $D_0(df/d\epsilon)(0)$ is zero, but there are several reasons to resist this conclusion. The data from previous experiments[11] on the frequency dependence of the flux at the point where $\nabla n_0=0$ require that there be a second term in the flux equation that is a function of frequency. Also, the theoretical origin[10] of this term seems fairly robust and reflects a mobility contribution to the transport. Finally, the efficacy of the rotating-

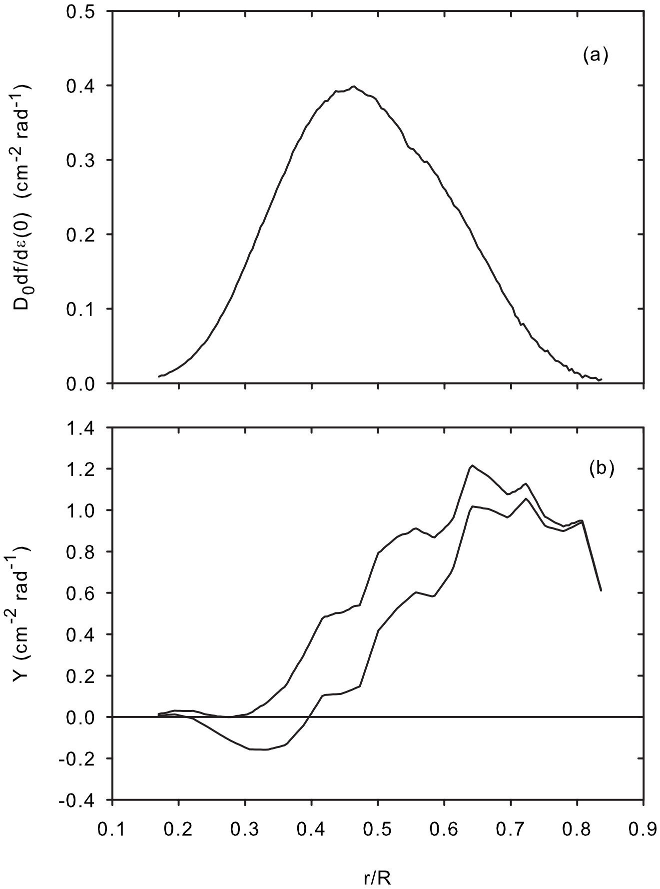

FIG. 6. (a) $D_0(df/d\epsilon)(0)$ as given by resonant particle theory [Eq. (11)] vs scaled radius r/R. (b) The effect of adding $D_0(df/d\epsilon)(0)$ to $(B/B_0)^{1.33}d(\Gamma-\Gamma_{sel})/d\epsilon$. The lower line shows the data of Fig. 4, $Y=(B/B_0)^{1.33}d(\Gamma-\Gamma_{sel})/d\epsilon$. The data has been interpolated to match to 256 radial positions of the $D_0(df/d\epsilon)(0)$ data. The upper line shows the same data with $D_0(df/d\epsilon)(0)$ added. In this case the former zero-crossing point at $r/R\approx 0.4$ no longer occurs.

wall technique[4,7] requires a term in the transport equation that can change sign with frequency (i.e., which is an odd power of ϵ).

It is interesting to note that if we introduce an *ad hoc* multiplicative factor $\eta<1$ to the $D_0(df/d\epsilon)(0)$ term, the zero-crossing correlation can be maintained and actually improved. This can be understood from Fig. 6. If we add a fraction of $D_0(df/d\epsilon)(0)$ to the original data, the upper curve in Fig. 6(b) will be shifted up by a lesser amount, with the result that the zero-crossing point will be shifted to the left to lower values of r/R. Referring to Fig. 5, we see that such an adjustment will move the data points down and improve the correlation for some of the data. Of course, if η is too large that the shift will make the correlation worse. We find that $\eta=0.15$ produces the best result with the standard deviation from a perfect correlation improving from $\sigma_{r/R}=0.024$ (for $\eta=0$) to 0.017. Values of η greater than 0.31 degrade the correlation, producing $\sigma_{r/R}$ values greater than 0.024.

So far we have drawn our conclusions solely from the correlation in the zero-crossings of the two sides of Eq. (12). We now examine the full set of $d(\Gamma-\Gamma_{sel})/d\epsilon$ versus r/R data and find parameter scalings in $(dD/d\epsilon)(0)$. When data was taken for various values of the center wire bias ϕ_{cw} and magnetic field B, the data points in Fig. 4 increased in magnitude with B and decreased with ϕ_{cw}. It also is apparent from this figure that the solid line data will have to be multiplied by an increasing function of radius to match the dot data. To quantify these scalings, we have assumed a power law dependence on r, B, and ϕ_{cw}, i.e.,

$$\frac{dD}{d\epsilon}(0)=C\left(\frac{r}{R}\right)^a\left(\frac{B}{B_0}\right)^b\Big/\left(\frac{\phi_{cw}}{\phi_0}\right)^c, \tag{13}$$

and adjusted the exponents a, b, and c and the multiplicative factor η through multiple regression to achieve the best correlation between the two sides of the equation

$$\left(\frac{B}{B_0}\right)^{1.33}\frac{d(\Gamma-\Gamma_{sel})}{d\epsilon}+\eta D_0\frac{df}{d\epsilon}(0)=-(\nabla n_0+f_0)\frac{dD}{d\epsilon}(0). \tag{14}$$

In Eq. (13), C is a constant to be determined and $\phi_0\equiv -140$ V. For the regression, we use the correlation coefficient r_{xy} as the figure of merit with $r_{xy}=1$ corresponding to perfect correlation.[14] The results of the regression for various cases are shown in Table I. The first case ("all free") gives the result when all four parameters (η, a, b, and c) were adjusted to give the largest value of r_{xy}. The next two columns give the result of fixing the value of η and adjusting a, b, and c. The final four columns give the results when all four parameters are fixed. In addition to r_{xy}, the table also

TABLE I. Results of regression analysis. In the first column, all four parameters (η, a, b, and c) were allowed to vary to maximize the correlation coefficient r_{xy}. The next two columns fix η and allow a, b, and c to vary. The last four columns show the results for certain fixed values of the parameters to give an indication of the sensitivity of r_{xy} to changes in the parameters.

Case →	All free	Fixed η	Fixed η	All fixed	All fixed	All fixed	All fixed
η	0.47	0	0.15	0.15	0.15	0.15	0.15
a	2.77	3.04	2.95	2	3	3	3
b	1.54	1.62	1.59	1	1	1.5	1.5
c	0.95	1.03	1.01	1	1	1.5	1
r_{xy}	0.929	0.916	0.923	0.877	0.900	0.902	0.922
Δr_{xy}	⋯	0.013	0.006	0.052	0.029	0.027	0.007
C (10^{-5} cm^2/rad)	0.384	0.365	0.371	0.363	0.585	0.294	0.384
σ_C/C (%)	1.61	1.75	1.67	2.17	1.94	1.91	1.61

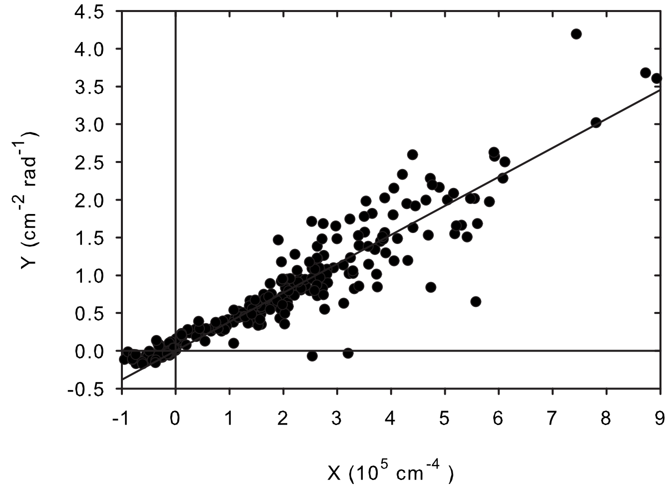

FIG. 7. Plot of the left side of Eq. (14), here abbreviated as Y, vs the right hand side (X) assuming the power law dependence given in Eq. (13) and using the values given in the first column of Table I. The correlation coefficient r_{xy} for this case is 0.929.

shows, for the last six cases, the change in r_{xy} with respect to the first column and the obtained value of the proportionality constant C and its fractional error σ_C/C. In Fig. 7 we plot all of our data (three values of ϕ_{cw} for each of four magnetic fields B) using the parameter values of the all free case, with the left side of Eq. (14) as the ordinate and the right side as the abscissa.

While the parameter values in the first column of Table I yield the best regression coefficient (0.932), the value of η is higher than the optimum value (0.15) for the zero-crossing correlation discussed previously. The remaining columns give an indication of the sensitivity of r_{xy} on the four parameters. The dependence on η is relatively weak and fixing $\eta=0.15$ to match the zero crossing correlation has only a minor effect on the regression coefficient. The dependence of r_{xy} on a, b, and c is stronger, as shown in the last four columns. A reasonable compromise between the zero-crossing results and the correlation results is given in the last column: $\eta=0.15$, $a=3$, $b=1.5$, and $c=1$. We note that these values are close to those that would be obtained if $(dD/d\epsilon)(0)$ was proportional to $(d\omega_R/dr)^{-1}$.

V. DISCUSSION

Our previous experiments[11] on the frequency dependence of the transport showed that the flux was a peaked function of the asymmetry frequency, but the requirement that $(dD/d\epsilon)(0)\neq 0$ excludes both the Gaussian and Lorentzian functions if they are centered at $\epsilon=0$. It does, however, allow such functions if they are centered at another point. For example, if $D(\epsilon)=\tilde{D}\exp[-(\epsilon-\alpha)^2/\beta^2]$, then

$$\frac{dD}{d\epsilon}(0)=\frac{2\alpha}{\beta^2}D(0). \tag{15}$$

Since $D(0)$ is nonzero, our requirement that $(dD/d\epsilon)(0)\neq 0$ is satisfied.

The observed dependence of $(dD/d\epsilon)(0)$ on B, ϕ_{cw}, and r seems to contradict the statement in our earlier work[12] that such dependencies have been removed by focusing on points where $\epsilon=0$. However, this statement refers to $D(0)$ and $f(0)$. The results can be harmonized by examining Eq. (15). If the frequencies α and/or β depend on B, ϕ_{cw}, and/or r, then $(dD/d\epsilon)(0)$ can as well, even if $D(0)$ does not.

The necessity of introducing the *ad hoc* multiplicative factor η in the second term of Eq. (14) is puzzling. Since this term has its origin in the radial derivative of the distribution function,[10] we speculate that this reflects the nonlinear modification of the distribution function by the applied asymmetry. Such an effect was recently documented in studies of electron acoustic waves in a Malmberg–Penning trap.[15]

Finally, we note that since our analysis is based on data in the vicinity of $\epsilon=0$, our constraints on $D(\epsilon)$ and $f(\epsilon)$ may not apply for large values of $|\epsilon|$. This could be the case if the physics in the vicinity of $\epsilon=0$ is different from that for other values of ϵ. Indeed, our simulation[16] of the particle dynamics in asymmetry-induced transport suggests that this may be so. We do not know of an analytic technique that would allow us, starting from Eq. (2), to determine from the data the two unknown functions $D(\epsilon)$ and $f(\epsilon)$ for all ϵ. We have tried to simply guess the functions that would fit the data, but without success.

VI. CONCLUSION

We have shown that further constraints can be placed upon $D(\epsilon)$ and $f(\epsilon)$ by comparing data near the $\epsilon=0$ points to a first order expansion of $\Gamma(\epsilon)$. The analysis revealed that $dD/d\epsilon(0)\neq 0$, in contradiction to resonant particle theory, and that $f(\epsilon)$ can only be a fraction of the size predicted by that theory. We have also shown that $dD/d\epsilon(0)$ exhibits a power-law scaling with radius, magnetic field, and the bias of the center conductor of the trap. These results provide a touchstone for future theoretical developments.

ACKNOWLEDGMENTS

This material is based on work supported by the Department of Energy under Award No. DE-FG02-06ER54882. The author acknowledges the assistance of Corrie Tate Smith in the initial stages of this work.

[1] J. H. Malmberg and C. F. Driscoll, Phys. Rev. Lett. **44**, 654 (1980).
[2] D. L. Eggleston, T. M. O'Neil, and J. H. Malmberg, Phys. Rev. Lett. **53**, 982 (1984).
[3] J. Notte and J. Fajans, Phys. Plasmas **1**, 1123 (1994).
[4] X.-P. Huang, F. Anderegg, E. M. Hollman, C. F. Driscoll, and T. M. O'Neil, Phys. Rev. Lett. **78**, 875 (1997).
[5] J. M. Kriesel and C. F. Driscoll, Phys. Rev. Lett. **85**, 2510 (2000).
[6] A. A. Kabantsev, J. H. Yu, R. B. Lynch, and C. F. Driscoll, Phys. Plasmas **10**, 1628 (2003).
[7] J. R. Danielson and C. M. Surko, Phys. Plasmas **13**, 055706 (2006).
[8] Y. Soga, Y. Kiwamoto, and N. Hashizume, Phys. Plasmas **13**, 052105 (2006).
[9] D. L. Eggleston, Phys. Plasmas **4**, 1196 (1997).
[10] D. L. Eggleston and T. M. O'Neil, Phys. Plasmas **6**, 2699 (1999).
[11] D. L. Eggleston and B. Carrillo, Phys. Plasmas **10**, 1308 (2003).
[12] D. L. Eggleston and J. M. Williams, Phys. Plasmas **15**, 032305 (2008).
[13] D. L. Eggleston and B. Carrillo, Phys. Plasmas **9**, 786 (2002).
[14] J. R. Taylor, *An Introduction to Error Analysis*, 2nd ed. (University Science Books, California, 1997), pp. 216–217.
[15] F. Anderegg, C. F. Driscoll, D. H. E. Dubin, T. M. O'Neil, and F. Valentini, Phys. Plasmas **16**, 055705 (2009).
[16] D. L. Eggleston, Phys. Plasmas **14**, 012302 (2007).